エッジ照明法を使ったX線位相コントラストイメージングの産業応用に関するニコン/UCL共同研究：新しい補完的な画像情報とサブピクセル特性の検出

松永教仁，矢野和弘，David BATE，Marco ENDRIZZI，Alessandro OLIVO

The Nikon/UCL collaboration on industrial applications of Edge-Illumination X-ray Phase Contrast Imaging: detection of new complementary information and of sub-pixel features

Norihito MATSUNAGA, Kazuhiro YANO, David BATE, Marco ENDRIZZI and Alessandro OLIVO

2012年以降，ニコンとユニバーシティ・カレッジ・ロンドン（以下，UCL）は，UCLが開発したエッジ照明法と呼ばれる通常の実験室サイズで運用可能な新しいX線位相コントラスト法について，共同研究を行っている．最近，その共同研究の焦点は，産業分野への応用に移行した．X線位相コントラスト法には3つの利点がある．1）従来のX線吸収イメージングでは視認できない被検物の詳細な構造を示すことができる．2）従来のX線吸収イメージングでは得られない補完的な画像コントラスト情報を提供することができる．3）暗視野像を利用することにより，装置解像度の限界を下回る被検物の詳細な構造を検出できる．この論文では，それらすべてについて例示する．特に，3）において，暗視野像が装置解像度よりも小さなスケールの微細構造情報（＝サブピクセル特性）を提供することが知られている．装置解像度よりも細かな溝が彫られた被検物を計測することにより，解像度限界を下回る微細構造も検出できることを示す．より一般的に，産業用途における複合材料の検査において有益な結果が得られる．また，英国研究・イノベーション機構UKRIによるProsperity Partnershipプログラムに採択されたことにより，エッジ照明法をより高いエネルギーにまで拡張できる機会を得た．これにより，高い原子番号の素材より成る厚めの被検物や，新たな積層造形（AM; アディティブ・マニュファクチャリング）分野への応用が可能になる．

Nikon and University College London (UCL) have collaborated since 2012 on of novel, laboratory-based X-ray Phase Contrast Imaging (XPCI) methods; recently, focus has shifted to industrial application. XPCI offers three advantages: 1) it reveals details invisible to conventional X-rays 2) it allows complementary contrast modalities 3) the dark field channel allows detecting details below the resolution limit of the imaging system. This paper presents examples of all three advantages, with emphasis on the third. Specifically on this latter aspect, it is known that dark field provides microstructural information on a scale smaller than the system's resolution. By using a micro-groove sample, we show that individual features below the resolution limit can also be detected. More generally, in industrial applications, important results have been achieved in the testing of composite materials, and the award of a "Prosperity Partnership" Program by United Kingdom Research and Innovation (UKRI) will enable extending XPCI to higher energies, allowing applications to high Z, thick samples and to the emerging field of additive manufacturing.

Key words 産業用非破壊検査，微細欠陥検出，X線イメージング，X線位相コントラスト，暗視野像
Industrial non-destructive inspection, Micro crack inspection, X-ray imaging, X-ray phase contrast, Dark field

1 INTRODUCTION

Since Wilhelm Röntgen's discovery of X-rays in 1895, X-ray imaging has been one of the few technologies that allow visualizing the internal structure of a sample non-destructively. In particular, X-ray Phase Contrast Imaging (XPCI) allows obtaining high contrast for samples presenting a weak X-ray attenuation, and as a consequence it has been actively studied over recent years. Several XPCI approaches have been developed to date, including free-space propaga-

tion (propagation-based imaging)[1)2)], Bonse-Hart interferometry (crystal interferometry)[3)4)], analyzer-based imaging (sometimes referred to as "Diffraction Enhanced" Imaging)[5)~7)], Talbot interferometry (grating-based imaging)[8)~10)] and edge illumination (EI, sometimes referred to as the "coded aperture" technique)[11)~13)]. Details on the various approaches can be found in a series of reviews that were recently published[14)15)].

Among those methods, Talbot interferometry and EI have attracted particular attention thanks to the possibility to implement them with extended sources, which is one of the key requirements in terms of translation from high-end synchrotron facilities to standard labs and, ultimately, commercial systems. Our collaboration focuses on EI, mostly because of its implementation not requiring source collimation[11)~13)], achromatic properties[16)], and robustness against vibrations[17)]. The edge illumination technique was first developed in Elettra Synchrotron of Italy in the late 1990s[18)]. Currently, many experimental results have been reported, mostly based around applications in biohealth and industrial fields[11)~13)]. These highlight the technique's potential in terms of application to market, within which hard X-ray dark field imaging with incoherent sample illumination[12)13)16)] can carve its own niche thanks to its ability to visualize various microstructures of the sample using laboratory scale systems, similarly to what has been demonstrated for dark field imaging in analyzer-based imaging[19)] or Talbot interferometry[20)]. So far, this dark field channel has been related to average microscopic sample features - namely sub-pixel structures averaged over one detector pixel[10)21)~23)]. Here, besides providing additional demonstration of its inherent complementarity to both the attenuation and the differential phase channels, we focus on single, isolated sub-pixel features, showing that these can be detected by the dark field channel down to sizes well below the inherent resolution limits of the imaging system. In EI, this resolution limit (referred to as δ_{RL} in the following to avoid repetitions) extends beyond the detector's intrinsic resolution, and is equal to the smallest between projected focal spot size (= real focal spot size multiplied by sample-to-detector distance and divided by source-to-sample distance) and aperture dimension in the pre-sample mask[24)]. We also show that this limit is mostly respected in the differential phase image, therefore corroborating the theoretical framework of ref. 24, while the dark field channel enables detecting finer isolated details.

2 IMAGING PRINCIPLE

Fig. 1 shows a schematic diagram of the EI XPCI system used in this demonstration experiment. The detector is a Hamamatsu C9732DK CMOS sensor with pixel size of 50 μm. The X-ray source is a rotating anode Rigaku MM007 with a molybdenum target. The tube voltage and current settings were 35 kVp and 25 mA respectively, and the focal spot size is approximately 80 μm. The pre-sample mask, manufactured by Creatv MicroTech (Potomac, MD) by electroplating gold on a patterned graphite substrate, had a period of 79 μm and an aperture width of 23 μm.

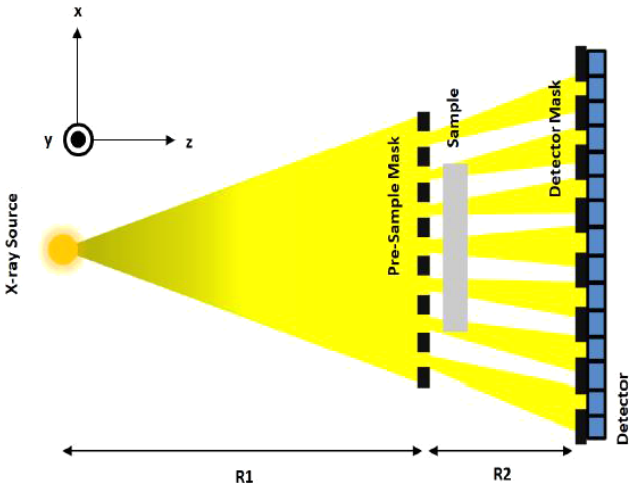

Fig. 1 Schematic representation of the laboratory-based edge-illumination X-ray imaging system used in this experiment.

The detector mask was fabricated in the same way and had a 98 μm period and 29 μm aperture width. The distances R_1 and R_2 between source and pre-sample mask and pre-sample mask and detector mask were of 1.6 m and 0.4 m, respectively which, when beam divergence is taken into account, leads to harmonic matching of the two masks. The detector itself is placed a few cm downstream of the detector mask, so that the 98 μm period of the latter projects into twice the pixel structure, leading to what we refer to as the "skipped" EI configuration[25)], used with indirect conversion detectors to reduce cross-talk between adjacent channels.

To extract the dark field signal, we start by measuring the "illumination" curve (IC) without a sample in place, i.e. the intensity variation observed at the detector when one mask (typically the pre-sample one), is scanned transversally (i.e. along x axis in Fig. 1). Fig. 2 schematizes the measurement method and highlights some key physical quantities of the IC. Following the introduction of a sample, the sample and the sample mask are moved rigidly in a series of points with respect to the stationary detector/detector mask assembly

(indicated as "System dithering" in Fig. 2(a)). The signal in the corresponding detector pixel is measured at each point, and a "sample in" IC is obtained by Gaussian fitting of the signals obtained at the various points. This fit $I_M(x)$ is then compared to the corresponding fit ($I_N(x)$) of the IC without the sample in place.

$$I_N(x) = \frac{t_N}{\sqrt{2\pi\sigma_N^2}} \exp\left[-\frac{(x-\Delta x_N)^2}{2\sigma_N^2}\right] + I_0, \quad (1)$$

$$I_M(x) = t_M\left[\frac{t_N}{\sqrt{2\pi\sigma_M^2}} \exp\left[-\frac{(x-\Delta x_M)^2}{2\sigma_M^2}\right] + I_0\right]. \quad (2)$$

The comparison between $I_M(x)$ and $I_N(x)$ allows extracting the attenuation, refraction and dark-field characteristics of the sample on a pixel-by-pixel basis. In particular, t_N, Δx_N, σ_N and I_0 in Eq. (1) are area, center, standard deviation and background value of the illumination curve without the sample. These values depend only on the characteristics of the imaging system, and are used as reference data to retrieve the sample parameters. t_M, Δx_M and σ_M in Eq. (2) are area ratio (relative area reduction), center and standard deviation of the illumination curve with the sample. These values represent the modification to the IC caused by absorption, refraction and USAXS in the sample. It is therefore possible to extract the absorption image t_M, the differential phase image Δx_M- Δx_N and the dark field (or USAXS) image σ_M^2 - σ_N^2 of the sample by measuring the IC with and without the sample in place[12)13)]. While this procedure yields the above three images sampled at a pitch equal to the detector pixel size, finer sampling pitches can be accessed by displacing the sample in sub-pixel steps ("Sample dithering" in Fig. 2(a)), repeating the above procedure at each step, and interleaving the obtained oversampled images (i.e. column 1 of dithering step 1, column 1 of dithering step 2, ⋯. column 1 of dithering step D, column 2 of dithering step 1 etc. if D dithering steps are used in total[25)]).

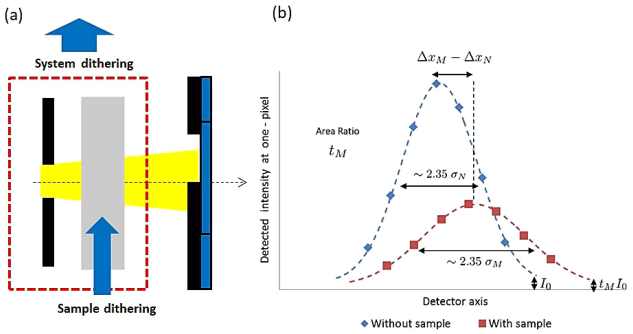

Fig. 2 (a) Schematization of the approach used to measure the illumination curve with and without the sample. "System dithering" indicates the translation in steps used to measure the illumination curve for each pixel, which is always repeated both with and without the sample. "Sample dithering" indicates an additional (optional) scan applied only to the sample, when this is sampled at a pitch finer than the pixel size. This allows accessing the ultimate resolution of the imaging system δ_{RL} as defined in the text. (b) shows example illumination curves measured with and without the sample, with the latter inducing curve broadening, intensity reduction and lateral shifts that allow extracting dark field, attenuation and refraction signals, respectively.

The ability of this procedure to yield a resolution beyond the pixel size limits is shown in Fig. 3, where the microstructure of coffee grains is highlighted in the phase image in Fig. 3(b) and confirmed by a scan of the same sample with an electron microscope (Fig. 3(c)). The attenuation image is shown in Fig. 3(a), which demonstrates the enhanced contrast provided by the phase channel; note that the two images were extracted from the same dataset according to Eqs. (1-2), and they thus have exactly the same X-ray statistics. This result also highlights that refraction (the integration of which yields the phase shift) and dark-field can be cast as line integrals, which makes 3D (computed tomography) acquisitions possible. Details can be found in references[26)~28)].

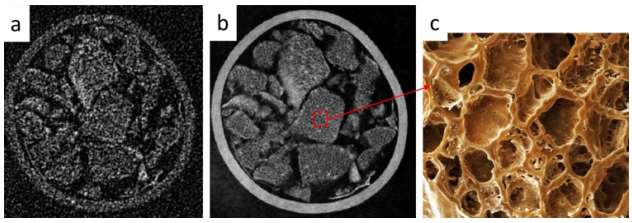

Fig. 3 Microstructure of coffee grains revealed by phase contrast (b), confirmed by al electron microscopy image of the same specimen (c). The figure also shows that conventional attenuation (a) provides much lower contrast at the same X-ray statistics.

3 EXPERIMENT

This paper presents additional data[29)] focusing on a sample specifically designed to assess the ability of the dark field image to detect individual sub-pixel features that are invisible to the other image channels. This consists of a series of microgrooves carved in a 2 mm thick acrylic substrate as shown in Fig. 4. Fig. 4(a) is a photograph of the sample, with the widest grooves clearly visible in the top right corner (highlighted by a dashed red circle). Fig. 4(b) is a schematic providing height and spacing between grooves, and the number coding we will use to refer to their individual width and depth. The depth of all grooves in the top group (1-8) is 10 μm, and their width ranges from 6 μm (groove 1 on the far left) to 200 μm (groove 8, far right). Grooves in the mid-

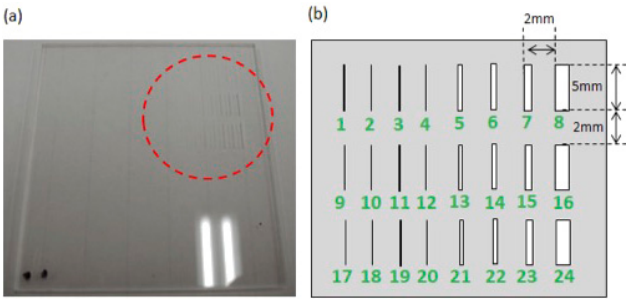

Fig. 4 (a) Photograph of the sample, with some grooves visible in the top right corner (dashed red circle) (b) schematic of the sample where grooves' height and separation are specified, and grooves are coded by numbers for ease of reference in the manuscript.

dle (9–16) and bottom (17–24) groups have the same width distribution, but depths of 50 μm and 100 μm respectively. Optical microscope imaging was used to obtain a more precise assessment of their width, e.g. grooves 17 and 18 (focus of the analysis of Fig. 5 below) had widths of 7.4 μm (as opposed to the design value of 6 μm) and 11.4 μm, respectively. All microgrooves were fabricated using the excimer laser technology.

This sample was imaged with the imaging system and parameters outlined above, and attenuation, differential phase and dark-field images were extracted by using the procedure of Eqs. (1–2). Details from the resulting images of grooves 17–24 (corresponding to the entire bottom line of the phantom) are shown in panels (a), (b) and (c) of Fig. 5, respectively. Horizontal profiles were extracted from each image, and these are reported in the same panel right above the corresponding images.

4 RESULTS AND DISCUSSION

As per the model described in ref. 24, we expect the spatial resolution δ_{RL} of the used EI system to be of the order of 20 μm, corresponding approximately to the projected focal spot and slightly smaller than the apertures in the pre-sample mask. We note that, while the detection of individual objects smaller than δ_{RL} cannot be excluded a priori (as is the case for any imaging system and its resolution), the results obtained from the attenuation and differential phase images, best appreciated in the plots above the images in of Fig. 5, are reasonably aligned with this coarse prediction. However, the visualization of finer details extends further in the dark field image, as visible from the image in Fig. 5(c) and even more clearly in the corresponding plot, where the additional detected details are highlighted by a dashed blue circle. Indeed, these details (17 and 18 in the numbered scheme of

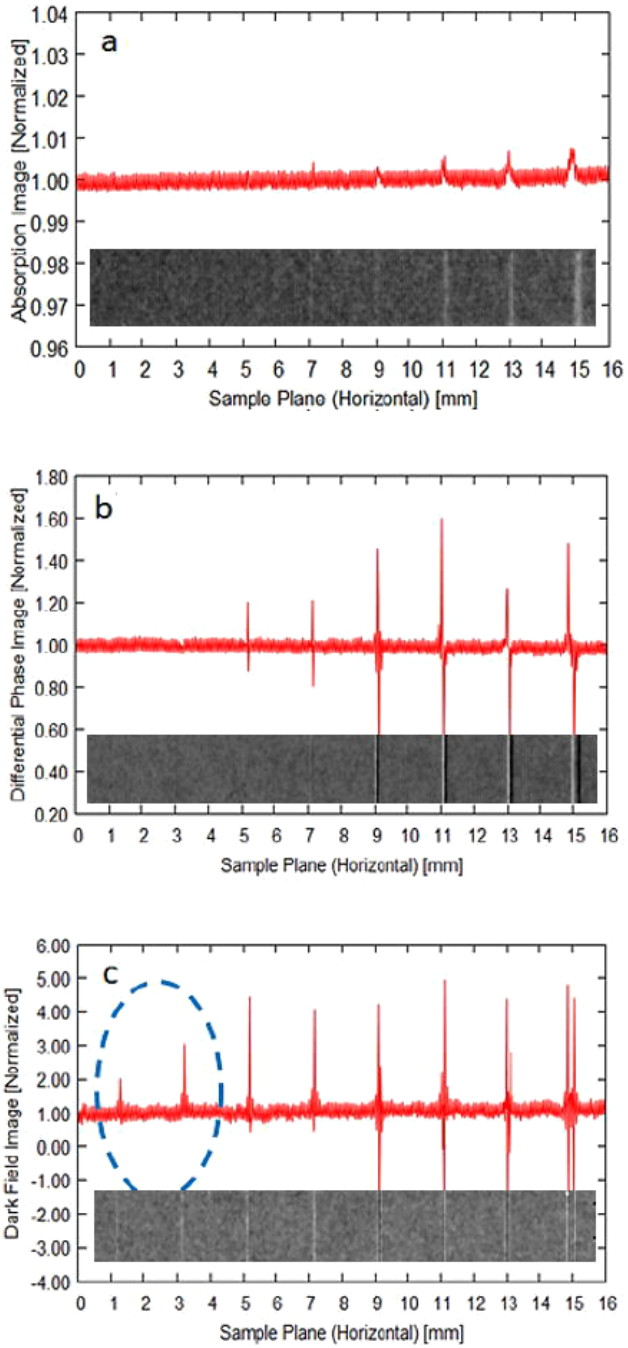

Fig. 5 Attenuation (a), differential phase (b) and dark field (c) images of grooves 17–24 (see Fig. 4(b)). Horizontal profiles were extracted from the images and are reported above all figures. A dashed blue circle in panel (c) highlights profiles of the thinnest grooves which, despite falling below the resolution limit of the imaging system δ_{RL} and indeed being invisible in the attenuation and differential phase images, are detected in the dark field image.

Fig. 4(b)) have a (measured) width of 7.4 μm and 11.4 μm respectively, therefore being significantly smaller than δ_{RL} in both cases.

As well as partly corroborating our previously developed theoretical framework, we find that these results are important, as they might suggest new application opportunities for

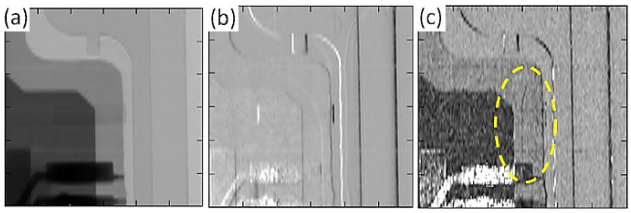

Fig. 6 Attenuation (a), differential phase (b) and dark field (c) images of part of the cracked SD card. The dashed yellow circle in (c) shows the crack, visible only in the dark field image.

the dark field imaging method. Alongside its ability to provide a signal proportional to the average concentration of sub-pixel structures, which has been repeatedly highlighted before[19)~23)], we observe here that dark field can also detect single, isolated features below the resolution limits of the imaging system, which are not picked up by the phase or attenuation channels. As a note of caution, it is important to stress that this sub-resolution detection potential depends on the sample characteristics, and in particular by the extent of the induced phase shifts, as made evident by the fact that the same fine features were not detected for the shallower grooves. This seems to indicate that it is the combination of size and signal strength that pushes a feature about the visibility threshold, an aspect that requires more detailed analysis to determine the effective bounds within which sub-resolution features are detected.

However, within these boundaries, this property may offer an opportunity to detect isolated defects or micro cracks on a scale which would not be accessible to other imaging modalities with the same level of resolution, which would find applications in non-destructive testing. As an example, Fig. 6(a)(b) and (c) show attenuation, differential phase and dark field images of a SD card with a crack respectively. A dashed yellow circle in Fig. 6(c) shows a cracked part can be seen only in the dark field channel. This result suggests that X-ray phase contrast imaging using edge illumination can be applied to non-destructive inspection of micro crack in industrial products such as electronic parts and processed fibers.

5 CONCLUSIONS AND OUTLOOK

The detection of individual sub-pixel features adds a string to the bow of an already powerful and versatile new imaging method, which recently proven transformative capabilities in the detection of damage in composite materials[30)] (Fig. 7).

At present, UCL and Nikon X-Tek Systems Ltd are working together to push the implementation of the multi-modal

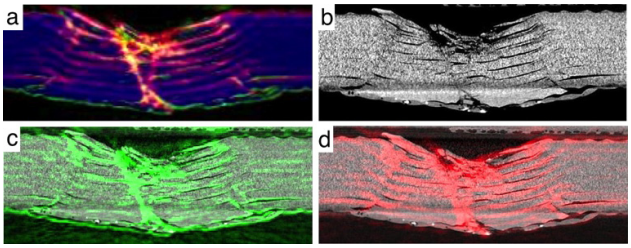

Fig. 7 Application of EI XPCI to cracks in composite materials. Panel (a) shows a "fused" image with attenuation in blue, refraction in green and dark-field in red, showing the complementarity of the channels as they emerge from different parts of the sample. Panel (b) shows a conventional micro CT for comparison. Panels (c) and (d) show an overlay of refraction and dark-field over the conventional micro-CT image, demonstrating detection of damage well beyond what can be revealed by conventional X-rays.

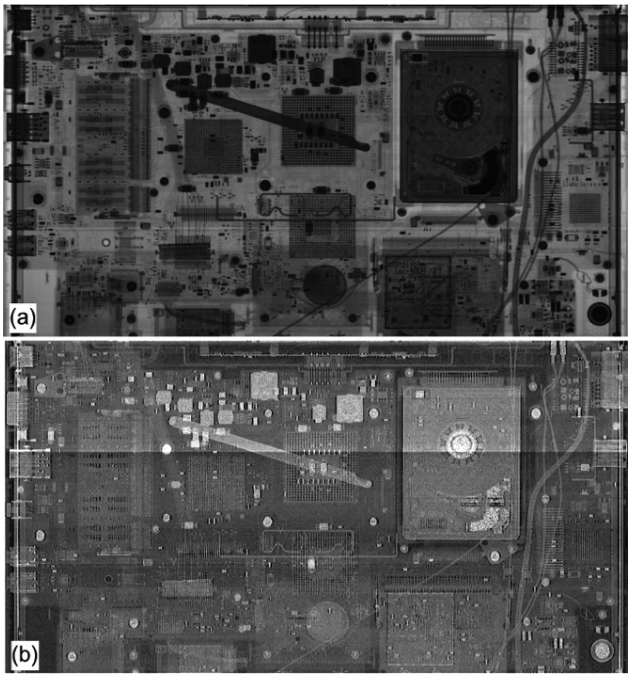

Fig. 8 Complementary images of a full laptop scanned at high X-ray energy – (a) attenuation and (b) dark-field.

X-ray methods to much higher X-ray energies. Feasibility at X-ray spectra up to 120 kVp has already been demonstrated, which enables for example the scan of a full laptop (Fig 8).

Concurrently, a pilot experiment on additive manufacturing has been conducted at the Diamond synchrotron light source in Oxfordshire, UK. Although data analysis is still underway, the ability of the dark field channel to detect small blemishes and unfused powders is already evident; once fully proven, this will be translated to conventional sources. Combining these advances with the new onesallowed by our 5-year prosperity partnership program makes us confident we will develop next-generation X-ray tools with

unprecedented capabilities for additive manufacturing and beyond.

Acknowledgements. This project was part supported by the UK Engineering and Physical Sciences Research Council Grant No. EP/I021884/1. M. E. and A. O. are supported by the Royal Academy of Engineering under the Research Fellowships and Chair in Emerging Technologies schemes, respectively.

REFERENCES

1) A. Snigirev, I. Snigireva, V. Kohn, S. Kuznetsov and I. Schelokov: "On the possibilities of x-ray phase contrast microimaging by coherent high-energy synchrotron radiation", *Rev. Sci. Instrum.*, **66** (1995), 5486.
2) S. W. Wilkins, T. E. Gureyev, D. Gao, A. Pogany and A. W. Stevenson: "Phase-contrast imaging using polychromatic hard X-rays", *Nature*, **384** (1996), 335.
3) U. Bonse and M. Hart: "AN X-RAY INTERFEROMETER WITH LONG SEPARATED INTERFERING BEAM PATHS", *Appl. Phys. Lett.*, **7** (1965), 99.
4) A. Momose: "Demonstration of phase-contrast X-ray computed tomography using an X-ray interferometer", *Nucl. Inst. and Meth. Phys. Res. A.*, **352** (1995), 622.
5) J. Davis, D. Gao, T. E. Gureyev, A. W. Stevenson and S. W. Wilkins: "Phase-contrast imaging of weakly absorbing materials using hard X-rays", *Nature*, **373** (1995), 595.
6) D. Chapman, W. Thomlinson, R. E. Johnston, D. Washburn, E. Pisano, N. Gmür, Z. Zhong, R. Menk, F. Arfelli and D. Sayers: "Diffraction enhanced x-ray imaging", *Phys. Med. Biol.*, **42** (1997), 2015.
7) I. Koyama, A. Momose, J. Wu, T. T. Lwin and T. Takeda: "Biological Imaging by X-ray Phase Tomography Using Diffraction-Enhanced Imaging", *Jpn. J. Appl. Phys.*, **44** (2005), 8219.
8) A. Momose, S. Kawamoto, I. Koyama, Y. Hamaishi, K. Takai and Y. Suzuki: "Demonstration of X-Ray Talbot Interferometry", *Jpn. J. Appl. Phys.*, **42** (2003), L866.
9) F. Pfeiffer, T. Weitkamp, O. Bunk and C. David: "Phase retrieval and differential phase-contrast imaging with low-brilliance X-ray sources", *Nat. Phys.*, **2** (2006), 258.
10) F. Pfeiffer, M. Bech, O. Bunk, E.F. Eikenberry, C. Brönnimann, C. Grünzweig and C. David: "Hard-X-ray Dark-Field Imaging Using a Grating Interferometer", *Nat. Mater.*, **7** (2008), 134.
11) A. Olivo and R. Speller: "A coded-aperture technique allowing x-ray phase contrast imaging with conventional sources", *Appl. Phys. Lett.*, **91** (2007), 074106.
12) M. Endrizzi, P. C. Diemoz, T. P. Millard, J. Louise Jones, R. D. Speller, I. K. Robinson and A. Olivo: "Hard X-ray dark-field imaging with incoherent sample illumination", *Appl. Phys. Lett.*, **104** (2014), 024106.
13) M. Endrizzi, B. I. S. Murat, P. Fromme and A. Olivo: "Edge-illumination X-ray dark-field imaging for visualising defects in composite structures", *Composite Structures*, **134** (2015), 895.
14) A. Olivo and E. Castelli: "X-ray phase contrast imaging: From synchrotrons to conventional sources", *Riv. Nuovo Cimento*, **37** (2014), 467.
15) M. Endrizzi: "X-ray phase-contrast imaging", *Nucl. Instrum. Meth. Phys. Res. A.*, **878** (2018), 88.
16) M. Endrizzi, F. A. Vittoria, G. Kallon, D. Basta, P. C. Diemoz, A. Vincenzi, P. Delogu, R. Bellazzini and A. Olivo: "Achromatic Approach to Phase-Based Multi-Modal Imaging With Conventional X-ray Sources", *Opt.Exp.*, **23** (2015), 16473.
17) T. P. Millard, M. Endrizzi, K. Ignatyev, C. K. Hagen, P. R. T. Munro, R. D. Speller and A. Olivo: "Method for automatization of the alignment of a laboratory based x-ray phase contrast edge illumination system", *Rev. Sci. Instrum.*, **84** (2013), 083702.
18) A. Olivo, F. Arfelli, G. Cantatore, R. Longo, R. H. Menk, S. Pani, M. Prest, P. Poropat, L. Rigon, G. Tromba, E. Vallazza and E. Castelli: "An Innovative Digital Imaging Set-Up Allowing a Low-Dose Approach to Phase Contrast Applications in the Medical Field", *Med. Phys.*, **28** (2001), 1610.
19) L. Rigon, H. J. Besch, F. Arfelli, R. H. Menk, G. Heitner and H.Plotow-Besch: "A new DEI algorithm capable of investigating sub-pixel structures", *J. Phys. D: Appl. Phys.*, **36** (2003), A107.
20) V. Revol, B. Plank, R. Kaufmann, J. Kastner, C. Kottler and A. Neels: "Laminate fibre structure characterisation of carbon fibre-reinforced polymers by X-ray scatter dark field imaging with a grating interferometer", *NDT and E Int.*, **58** (2013), 64.
21) S. K. Lynch, V. Pai, J. Auxier, A. F. Stein, E. E. Bennett, C. K. Kemble, X. Xiao, W.-K. Lee, N. Y. Morgan and H. Wen: "Interpretation of dark-field contrast and particle-size selectivity in grating interferometers", *Appl. Opt.*, **50** (2011), 4310.
22) T. P. Millard, M. Endrizzi, L. Rigon, F. Arfelli, R. H. Menk, J. Owen, E. Stride and A. Olivo: "Quantification of microbubble concentration through x-ray phase contrast imaging", *Appl. Phys. Lett.*, **103** (2013), 114105.
23) P. Modregger, M. Kagias, S. C. Irvine, R. Brönnimann, K. Jefimovs, M. Endrizzi and A. Olivo: "Interpretation and Utility of the Moments of Small-Angle X-Ray Scattering Distributions", *Phys. Rev. Lett.*, **118** (2017), 265501.
24) P. C. Diemoz, F. A. Vittoria and A. Olivo: "Spatial resolution of edge illumination X-ray phase-contrast imaging", *Opt. Exp.*, **22** (2014), 15514.
25) K. Ignatyev, P. R. T. Munro, R. D. Speller and A. Olivo: "Effects of signal diffusion on x-ray phase contrast images",

Rev. Sci. Instrum., **82** (2011), 073702.

26) C. K. Hagen, P. R. T. Munro, M. Endrizzi, P. C. Diemoz and A. Olivo: "Low-dose Phase Contrast Tomography With Conventional X-Ray Sources", *Med. Phys.*, **41** (2014), 070701.

27) F. A. Vittoria, M. Endrizzi, G. K. Kallon, C. K. Hagen *et al.*: "Multimodal Phase-Based X-Ray Microtomography with Nonmicrofocal Laboratory Sources", *Phys. Rev. Appl.*, **8** (2017), 064009.

28) M. Endrizzi, F. A. Vittoria, L. Rigon, D. Dreossi *et al.*: "X-ray Phase-Contrast Radiography and Tomography with a Multiaperture Analyzer", *Phys. Rev. Lett.*, **118** (2017), 243902.

29) N. Matsunaga, K. Yano, M. Endrizzi and A. Olivo: "Detection of individual sub-pixel features in edge-illumination x-ray phase contrast imaging by means of the dark-field channel", *J. Phys. D: Appl. Phys.*, **53** (2020), 095401.

30) D. Shoukroun, L. Massimi, F. Iacoviello. M, Endrizzi, D. Bate *et al.*: "Enhanced composite plate impact damage detection and characterisation using X-Ray refraction and scattering contrast combined with ultrasonic imaging", *Compos. B.*, **181** (2020), 107579.

松永教仁
Norihito MATSUNAGA
研究開発本部
光技術研究所
Optical Research Laboratory
Research & Development Division

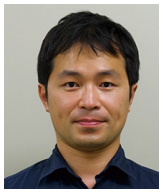

矢野和弘
Kazuhiro YANO
研究開発本部
光技術研究所
Optical Research Laboratory
Research & Development Division

David BATE
Nikon X-Tek Systems Ltd

Marco ENDRIZZI
University College London

Alessandro OLIVO
University College London